Sensors & Diagnostics

PAPER

View Article Online
View Journal | View Issue

Check for updates

Cite this: *Sens. Diagn.*, 2025, **4**, 202

Optimizing the preparation of laser-derived 3D porous graphene electrodes for modification-free sensing of heavy metal ions†

Ismaila Diédhiou, [ab] Amal Raouafi, [b] Sami Hamzaoui,[c] Modou Fall [a] and Noureddine Raouafi *[b]

Heavy metallic cations are prevalent in the environment and have detrimental effects on human health and flora. Research into methods for their detection is increasing. Laser-derived graphene electrodes (LDGEs) have gained popularity in electrochemical applications owing to their straightforward preparation, cost-effectiveness, porous structure, high specific surface area, and advantageous electronic properties. In this study, we showed that the fine-tuning of laser beam parameters, such as power and speed, as well as the electrochemical detection parameters, allowed detecting heavy metal ions, specifically Cd^{2+} and Pb^{2+}, using carefully optimized porous LDGEs, without the need of adding any other metals such as Bi^{3+}. The optimal LDGEs, respectively fabricated with a laser power and speed of 6.4 W and 30 cm s^{-1} were characterized using electrochemical measurements, digital imaging, scanning electron microscopy, and Raman spectroscopy, confirming the 3D porous structure. The LDGEs were then subjected to square-wave anodic stripping voltammetry for the simultaneous detection of Cd^{2+} and Pb^{2+} in a 0.1 M acetate-buffered solution at pH 4. The key metrics for the LDGE-based sensor were as follows: sensitivities of 0.45 (Cd^{2+}) and 0.93 (Pb^{2+}) μA ppb^{-1} cm^{-2}, linear ranges spanning from 25 to 1000 ppb (Cd^{2+}) and 10 to 500 ppb (Pb^{2+}), and detection limits of 6.13 ppb (Cd^{2+}) and 2.96 ppb (Pb^{2+}) (at S/N = 3).The electrochemical sensor could simultaneously detect Cd^{2+} and Pb^{2+} in real samples, including ore and tap water. This underscores the applicability and versatility of the optimized LDGEs for heavy-metal ion detection in complex environmental matrices.

Received 22nd August 2024,
Accepted 12th January 2025

DOI: 10.1039/d4sd00290c

rsc.li/sensors

Open Access Article. Published on 16 January 2025. Downloaded on 4/26/2026 5:57:25 PM.
This article is licensed under a Creative Commons Attribution-NonCommercial 3.0 Unported Licence.

1. Introduction

Anthropogenic activities, such as the extensive use of chemicals in agriculture, industrial waste, and wastewater treatment, contribute to the release of diverse pollutants, including heavy metals and other inorganic and organic pollutants, into the environment.[1,2] This contamination poses a threat to water resources and food[3] because heavy metal ions, such as cadmium, lead, mercury, arsenic, cobalt, chromium, and copper, are highly toxic, stable, and non-biodegradable.[4] Their presence in the ecosystem is widespread, impacting environmental and ecological processes and correlating with severe health issues, including cancer and dysfunction of the nervous, genital, bone marrow, and kidney systems.[5]

Recognizing their detrimental effects, international organizations such as WHO, FDA, CDC, EPA, and WFD have established stringent guidelines to limit pollutant levels in water. For instance, the WHO has set the maximum concentration limit for cadmium in drinking water to 5 ppb, and the WFD has reduced the limit for lead cations from 10 ppb to 5 ppb.[6] Hence, it is imperative to develop simple methods to detect and quantify heavy metal ions in water. Electrochemical techniques stand out because of their simplicity, cost-effectiveness, speed, high sensitivity, and ease of miniaturization.[7,8] Among the electrochemical techniques, anodic stripping techniques, specifically differential pulse anodic stripping voltammetry[9,10] and square wave anodic stripping voltammetry, are widely employed for heavy metal ion electroanalysis by the electrochemical reoxidation of previously electrochemically reduced metal ions on the electrode surface.[11,12] These techniques offer advantages, such as cost-effectiveness, speed, absence of laborious samples, and suitability for on-site measurements.[13–15] They

[a] *Laboratory of Organic Physical Chemistry and Environmental Analyses, Department of Chemistry, Faculty of Sciences and Techniques, Cheikh Anta Diop University, Dakar, Senegal*
[b] *Laboratory of Analytical Chemistry and Electrochemistry (LR99ES15), Department of Chemistry, Faculty of Science, University of Tunis El Manar, Tunis, 2092 Tunis El Manar, Tunisia. E-mail: noureddine.raouafi@fst.utm.tn*
[c] *Department of Radiologic Technology, College of Applied Medical Sciences, Qassim University, P.O. Box 6666, Buraydah 51452, Saudi Arabia*
† Electronic supplementary information (ESI) available. See DOI: https://doi.org/10.1039/d4sd00290c

© 2025 The Author(s). Published by the Royal Society of Chemistry

Open Access Article. Published on 16 January 2025. Downloaded on 4/26/2026 5:57:25 PM. This article is licensed under a Creative Commons Attribution-NonCommercial 3.0 Unported Licence.

are used not only for the detection of heavy metal ions but also for the electrochemical sensing of small molecules, such as glucose,[16–18] antibiotics,[19] pesticides,[20–22] hormones,[23] analgesics,[24] *etc.*

Using lasers for localized carbonization, particularly for commercial polymers such as polyimide, is an emerging technique for the fabrication of functional graphene-like nanocarbons.[25–29] This direct laser-derived graphene fabrication method presents a compelling alternative to traditional printing technologies, offering advantages in terms of efficiency, eco-friendliness and cost-effectiveness.[30,31] The morphologies of laser-derived graphene, including fiber-like structures, isotropic or anisotropic porous structures, and cellular network-shaped structures, can be tailored by adjusting laser parameters.[32] Rapidly, a large plethora of applications were devised for these electrodes such as piezoresistive and pH sensors,[33] sensors for small bioactive molecules[34] such as nitrite,[35] dopamine,[36,37] paracetamol,[38–41] glucose,[42] and amoxicillin,[43] gas sensors,[44] and supercapacitors.[26,45,46]

Traditionally, heavy metal ions have been detected using electrodes modified with conductive polymers,[47–49] or nanoparticles.[50,51] Electrodes modified with reduced graphene oxide have also been used to detect heavy metals.[52,53] Although these approaches can provide large detection ranges and low detection limits, they require at least two preparation steps. Laser-derived graphene electrodes are a cost-effective alternative and are prepared in one laser writing step. The combined cost of polyimide tape and polyethylene terephthalate does not exceed $18, and a single roll of polyimide tape can produce up to 6000 electrodes, resulting in an estimated cost of less than $0.01 per electrode (*i.e.* 3 electrodes for $0.01). For instance, Liu *et al.* used laser-derived graphene to detect Pb^{2+} in range from 1 to 100 μg L^{-1} with a limit of detection of 0.5 μg L^{-1}.[54] Jeong *et al.* prepared laser-derived fiber electrodes from the laser irradiation of a polyimide film with high laser power (46 J cm^{-2}), which were used for the detection of both Cd^{2+} and Pb^{2+} after the deposition of bismuth nanoparticles.[55] The dynamic range and detection limit were 1.0 to 140.0 μg L^{-1} and 0.4 μg L^{-1} (S/N = 3), respectively. The same research group also reported a silver nanoparticle/laser-derived graphene electrode for the simultaneous detection of Cd^{2+}, Pb^{2+}, and Cu^{2+} using the SWASV technique. The sensor had a dynamic range of 0.0 to 120.0 μg L^{-1} and a detection limit of 0.1 μg L^{-1}.[56] In another study, a laser-derived graphene electrode was modified with SnO_2 and CeO_2 nanoparticles and subsequently coated with poly(sulfanilic acid) through electrochemical polymerization to detect Cd^{2+} ions using differential pulse anodic stripping voltammetry.[57] Under optimal conditions, the electrode showed a broad linear concentration range (0.1–160 μg L^{-1}) with a low detection limit of 0.01 μg L^{-1}.

In this study, we present the straightforward fabrication of LDGE and its application as a high-performance electrode for the simultaneous detection of cadmium and lead ions, without the addition of other nanoparticles, making a novel contribution to the field. LDGEs were fabricated using the optimized laser parameters, and their formation was confirmed by scanning electron microscopy, energy dispersive X-ray spectroscopy, and Raman spectroscopy. These were used to simultaneously detect Cd^{2+} and Pb^{2+} using square-wave anodic stripping voltammetry. We investigated the effects of the measurement conditions, optimized the SWASV parameters, and determined the sensitivity, detection limit, repeatability, and reproducibility. Even though the electrode constitution can impact these electroanalytical parameters, it appears that DPASV has the advantage of leading to lower detection limits, but SWASV is more sensitive. This is why we chose the SWASV technique. Finally, LDGEs were applied to measure the concentrations at ten nanomolar level of Cd^{2+} and Pb^{2+} in the real samples like tape water and water sample from ore.

2. Experimental

2.1. Apparatuses

A Raman spectrometer (LAB-RAM HR 800, Horiba, USA), scanning electron microscope (JSM-7900F SEM), and Bruker DektakXT stylus profilometer (MA, USA) were used to characterize the laser-derived graphene electrodes and assess their structural properties. The SEM instrument was equipped with an energy-dispersive X-ray elemental analyzer. We employed a digital microscope (G1200 Electronic Microscope 1200×) with a maximum magnification of 12 MP to capture the digital images of the laser-derived graphene electrodes. The electrodes were fabricated using a laser cutter/engraver of 40 W power (Shenzhen, China). Graphene is formed by laser burning the polyimide film bonded to polyethylene, as shown in Scheme 1.

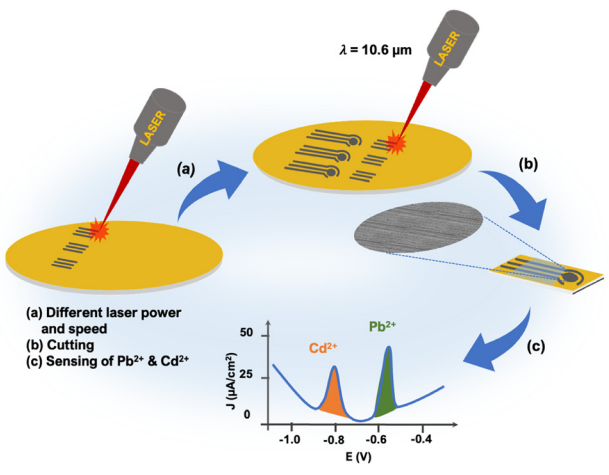

Scheme 1 Schematic illustration of the fabrication of laser-derived graphene electrodes using direct laser scribing on polyimide (yellow portion) and their applications: (a) direct laser writing, (b) cutting and insulating electrodes, and (c) anodic stripping voltamperograms recorded in presence of cadmium and lead ions.

Open Access Article. Published on 16 January 2025. Downloaded on 4/26/2026 5:57:25 PM. This article is licensed under a Creative Commons Attribution-NonCommercial 3.0 Unported Licence.

All electrochemical measurements were performed using a PalmSens4 potentiostat (The Netherlands). A three-electrode configuration (see Scheme 1) consisting of a counter electrode, a working electrode (diameter = 5 mm corresponding to geometrical surface area of 0.196 cm^2 for all working electrodes), and a pseudo-reference in graphene was used for the electrochemical measurements. The electrochemical characterization of LDGE was performed using cyclic voltammetry and electrochemical impedance spectroscopy, while heavy metal ion detection was performed using the SWASV technique. The pH values of the different solutions were determined using a Metrohm 744 pH meter.

2.2. Chemicals and reagents

Hydrochloric acid (37%), acetic acid (99.8%), perchloric acid (70%), sodium acetate (99%), absolute ethanol (≥99.8%), lead nitrate (98%), and cadmium nitrate tetrahydrate (98%) were purchased from Sigma-Aldrich (Germany). Sodium hydroxide (98%) and potassium chloride (99+%) were purchased from Acros Organics (Belgium). Commercial polyimide (PI) tape (thickness = 125 μm) was purchased from 3M (MA, USA). All reagents were used as received.

Acetic acid and sodium acetate were used to prepare an acetate-buffered solution, while HCl (1.0 M) and NaOH (1.0 M) were used to adjust the ABS pH to the desired value. Distilled water was used to prepare all solutions. Heavy metal reagents are in salt form. They are less toxic, but just as dangerous, which is why we use these reagents with great care in the laboratory, and with all safety features during experimental procedures.

2.3. Fabrication of laser-derived graphene electrodes

For the production of laser-derived graphene electrodes, a polyimide tape (yellow portion in Scheme 1) surface was carefully affixed to the PET substrate to prevent the formation of cracks on the surface of the LDGE electrodes, which were subsequently subjected to direct laser writing. Before lasing, the *z*-distance was set as 21 mm. Different power percentages (10–20% of 40 W) and laser beam speeds ranging from 10 to 50 cm s^{-1} were used to scribe the electrodes.

2.4. Electrochemical measurements

2.4.1. Electrochemical characterizations. Electrochemical characterizations of the LDGE6.4W30 electrode using CV and EIS were conducted using a 5 mM hexacyanoferrate(III/II) redox probe, dissolved 0.1 M KCl solution. Following activation of the LDGE6.4W30 electrode with NaOH 0.1 M solution using CV at a high scan rate of 400 mV s^{-1}, 80 μL of the redox probe solution was applied to the surface of the LDGE6.4W30 electrode for characterization using either CV or EIS.

For the CV electroactivity study, the scan rate was maintained at 100 mV s^{-1}. In the case of the EIS method, the characterization was performed using the same redox probe, with a potential applied during measurement (E_{dc}) set at 0.0 V, a potential amplitude of 5 mV, and a frequency range from 100 kHz to 0.1 Hz. This frequency range corresponds to 43 or 7 points per decade.

2.4.2. Electrochemical detection conditions. The electrochemical detection of heavy metal ions was performed using SWASV in a 0.1 M acetate buffer solution. The conditioning potential, step potential, and amplitude potential were set at 0.5 V, 5 mV, and 50 mV, respectively, for all detection measurements. The conditioning time (time during which the conditioning potential was applied) and equilibration time were standardized to 10 s and 30 s, respectively, for all detection measurements. The optimized detection parameters are described in section 3.5.

3. Results

3.1. Choice of the laser scribing parameters

3.1.1. Laser power. The laser power was optimized by assessing the electroanalytical response of the laser-derived graphene electrodes in the presence of 500 ppb Pb^{2+} in a 0.1 M acetate buffer solution at pH 4. While maintaining the *z*-distance unchanged, we explored the laser power across a range from 4.0 to 8.0 W, in 0.8 W increments, with the laser speed in the *xy*-plane set at 40 cm s^{-1}. Fig. S1† displays the anodic square-wave voltammograms, and Fig. 1A illustrates the peak current densities plotted against power.

At a power of 4.0 W, minimal carbonization occurred on the PI film, resulting in faint burn traces, and an electrode, LDGE4.0W40, did not yield satisfactory SWASV responses (see the first image in Fig. 3A). Conversely, at 8.0 W, severe damage occurred to the electrode, including to the PET underlayer. Fibrous structures resembling thorns were observed at 8.0 W, leading to the formation of LDGE8.0W40, which exhibited a poor electroanalytical response due to the collapse of surface fibers upon the deposition of sample drops, rendering the electrode surface muddy and poorly conductive. Laser powers of 4.8 W and 5.6 W resulted in relatively weak electroanalytical responses for lead detection. However, at 7.2 W power, the LDGE7.2W40 electrode exhibited an average SWASV response for lead detection. The highest electroanalytical response was achieved with the LDGE6.4W40 electrode scribed at a laser power of 6.4 W and a laser speed of 40 cm s^{-1}. This important response is due to the porous structures of LDGE6.4W40. This optimal power value was used for the subsequent optimization of the laser scanning speed.

3.1.2. Laser speed. Laser speed was optimized under the same conditions as stated before, with the laser beam power set at 6.4 W and the scanning speed varied from 10 to 50 cm s^{-1} in increments of 10 cm s^{-1}. Fig. S2† illustrates the square-wave anodic stripping voltammograms of Pb^{2+} ions, and the histogram in Fig. 1B shows the peak current densities plotted against the laser scanning speed.

Using the LDGE6.4W10 electrode at a laser scanning speed of 10 cm s^{-1} resulted in a very weak electrochemical

© 2025 The Author(s). Published by the Royal Society of Chemistry

Open Access Article. Published on 16 January 2025. Downloaded on 4/26/2026 5:57:25 PM.
This article is licensed under a Creative Commons Attribution-NonCommercial 3.0 Unported Licence.

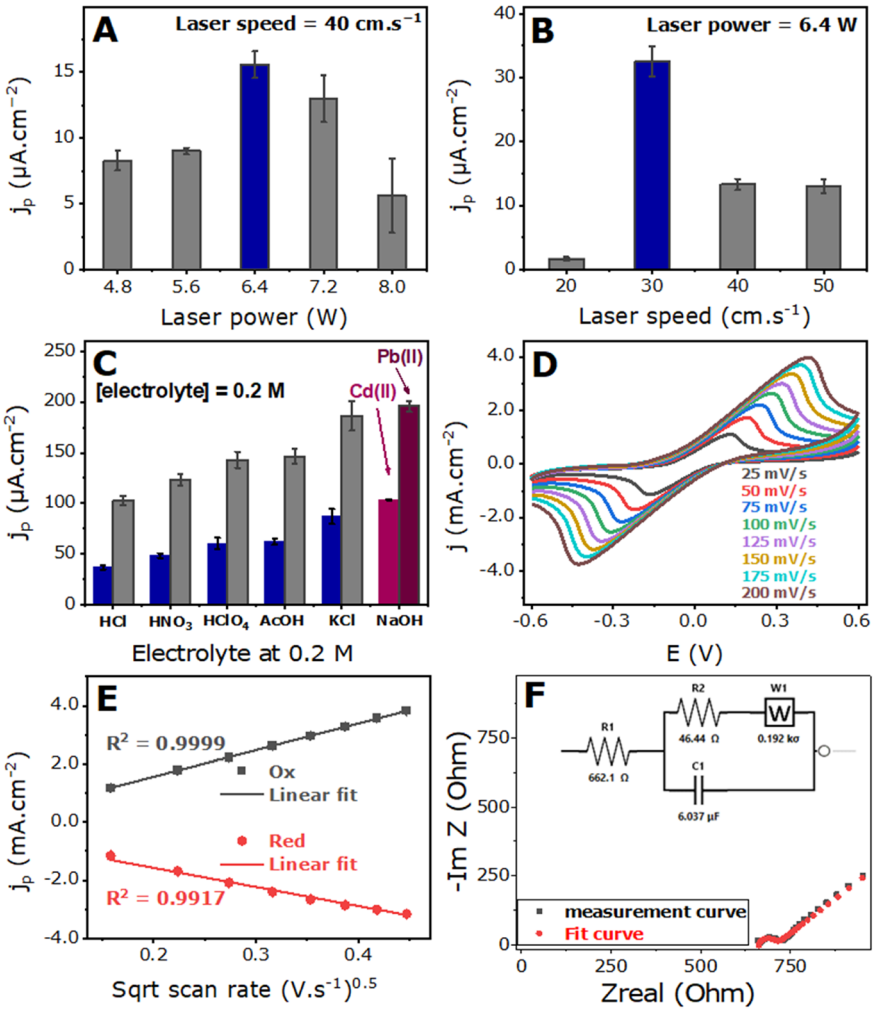

Fig. 1 Optimization of LDGE electrode fabrication and kinetic characteristics. Histograms of the SWASV responses for 500 ppb Pb^{2+} as a function of (A) laser power and (B) laser speed. Selection of activation electrolyte (C). Electroactivity of the LDGE6.4W30 electrode in 5 mM equimolar hexacyanoferrate(III/II) dissolved in KCl 0.1 M (D), calibration curve of j_p as a function of the square root of scan rate and their linear fits (E), Nyquist plot of LDGE6.4W30 recorded in 5 mM hexacyanoferrate(III/II) (F).

signal owing to the extensive damage to the electrode materials at this combination of laser power and speed. Similarly, a low electrochemical response is observed at 20 cm s^{-1}. The most favorable electrochemical response was obtained at 30 cm s^{-1}, because this speed is moderate for give a very good porous structures, whereas the responses began to decrease at laser speeds of 40 and 50 cm s^{-1}. At these higher laser scanning speeds, the limited exposure time of the polymer to the laser is insufficient to induce an adequate quantity of graphene. These speeds are too fast. Consequently, the LDGE6.4W30 electrode was selected as the optimal choice for further electroanalytical studies.

3.2. Activation electrolyte

To investigate the effect of electrolytes on the activation of laser-derived graphene electrodes, we examined various supporting electrolytes, all prepared at the same concentration of 0.2 M. Activation was performed using cyclic voltammetry by potential sweeping from −1 to +1 V at a scan rate of 0.4 V s^{-1} for 50 cycles. Subsequently, the activated electrodes were used to detect Pb^{2+} and Cd^{2+} ions, each at a concentration of 500 ppb dissolved in an acetate-buffered solution. The voltammograms are shown in Fig. S3† and the peak current densities are shown in the histogram in Fig. 1C.

The results indicated that the current densities increased with the strength of the acidic electrolytes and decreased with weakly acidic electrolytes, such as acetic acid. Furthermore, the current densities of the peak oxidation are even higher in neutral electrolytes, such as potassium chloride, and stronger in basic electrolytes, such as sodium hydroxide. Consequently, NaOH was chosen as the electrolyte for the activation of the laser-derived graphene electrodes. This result is due to the fact that NaOH is very effective for the electrochemical polishing of vitreous carbon electrodes; consequently, it is likely also effective for LDGEs, as confirmed by the results.

Open Access Article. Published on 16 January 2025. Downloaded on 4/26/2026 5:57:25 PM.
This article is licensed under a Creative Commons Attribution-NonCommercial 3.0 Unported Licence.

Notably, in other studies,[36,38] certain LDGEs or carbon-printed electrodes were activated using neutral or slightly basic phosphate buffer solutions. We believe that the optimal choice of activation electrolyte for these LDGEs depends on the nature of the platform they accommodate, that is, the type of sensor (chemical or biological) being fabricated. Therefore, electrolyte selection should be aligned with the specific requirements of these electrodes.

It is essential to investigate the influence of electrolyte solution pH and pK_a on the current densities of metal oxidation peaks (Fig. 2). Consequently, the cumulative current densities of both cadmium(II) and lead(II) were plotted against the pH and pK_a of the activating solutions. The results demonstrated an increase in the current densities as acidity decreased (Fig. 2A) and pK_a values increased (Fig. 2B), suggesting that neutral or basic media are better for the activation of freshly prepared LDGEs.

3.3. Electrochemical characterizations

3.3.1. Using cyclic voltammetry. The electrochemical characterization of LDGE6.4W30 was performed in a redox solution of hexacyanoferrate(III/II) at a concentration of 5 mM prepared in a 0.1 M KCl electrolytic solution. The electroactivity of the LDGE6.4W30 electrode was studied by cyclic voltammetry, sweeping the potential between −0.6 and +0.6 V and varying the scan rate from 25 to 200 mV s^{-1}.

Fig. 1D illustrates a clear increase in the peak current density with increasing scan rate. Furthermore, Fig. 1E shows the linear relationship between the peak current densities and square root of the scan rates, exhibiting high linear correlation coefficients (R^2 = 0.999 and R^2 = 0.992) for the oxidation and reduction peaks, respectively. This suggests that the kinetics are governed by the diffusion of the electroactive species in the solution toward the electrode active surface.[58]

3.3.2. Using electrochemical impedance spectroscopy. The electrochemical performance of the electrode was further studied using electrochemical impedance spectroscopy with the same redox probe in the frequency range of 100 kHz to 0.1 Hz. As shown in Fig. 1F, the Nyquist plot consists of a semicircle (at high frequencies) followed by a 45° slope segment at low frequencies, indicating the presence of charge-transfer resistance (R_{ct}) and Warburg capacitance (W) related to the diffusion of redox species to the electrode surface. A Randles electrical equivalent circuit was used to fit the experimental data, demonstrating a low R_{ct} value of 46.44 Ω. We estimated R_{ct} by using Circuit fitting tab in PSTrace setup (see Table 1). This allows us to deduce the parameters of the Nyquist curve. This low R_{ct} value was comparable to that measured using a low-cost multimeter (Fig. S4†). Despite these variations, these consistently low values provide valuable insights into the excellent electron transfer performance of $[Fe(CN)_6]^{3-/4-}$ on the electrode surface.[59]

3.4. Microscopic and spectroscopic characterizations

3.4.1. Morphologic characterizations. Fig. 3 shows the physicochemical characteristics of the prepared electrodes. Fig. 3A shows digital images of all laser-derived graphene electrodes recorded at a magnification of 1200×, providing an initial glimpse of their surfaces. As demonstrated by electrochemical measurements, the best response is obtained at a combination of laser power and speed of 6.4 W and 30 cm s^{-1}. For a more detailed view, the SEM image displayed in Fig. 3B clearly reveal the three-dimensional porosity of the graphene structures of the LDGE6.4W30 electrode. Pores of 2–5 μm are visible in the higher-magnification image.

The elemental composition was determined by EDX elemental analysis (Fig. S5†) showed the presence of 92.1%, 1.7%, and 6.2% carbon, nitrogen, and oxygen, respectively, arising from the carbonization of the polyimide membrane.

The 3D optical profilometer image in Fig. 3C shows an area of 4 mm^2 on the LDGE6.4W30 electrode, confirming its rough 3D surface structure. The depicted patterns exhibit heights ranging from −100 μm to +100 μm, which roughly corresponds to a width of the laser beam of ∼100 μm. The LDGE carbon layer thickness of the working electrode was ∼200 μm.

3.4.2. Raman spectroscopy. Raman spectra recorded for the polyimide film before and after laser irradiation (Fig. 3D). The spectrum of the polyimide film shows several peaks located at 980–1350, 1615, and 1725 cm^{-1}, and the region of 2800–3100 cm^{-1} can be assigned to the modes of organic functional groups. The LDGE spectrum displays three major peaks, the first one (D peak) appearing at

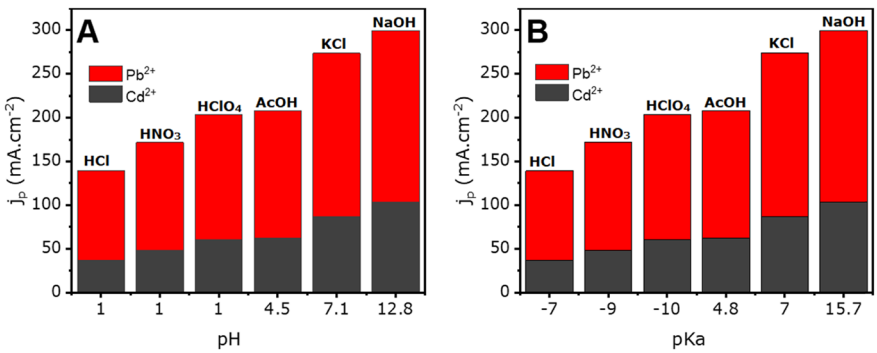

Fig. 2 Plot of the pH values (A) and (B) of the electrolytic solution *vs.* the cumulative peak current densities for Cd^{2+} and Pb^{2+}.

© 2025 The Author(s). Published by the Royal Society of Chemistry

Open Access Article. Published on 16 January 2025. Downloaded on 4/26/2026 5:57:25 PM.
This article is licensed under a Creative Commons Attribution-NonCommercial 3.0 Unported Licence.

Table 1 Electrochemical impedance spectroscopy of parameters values

Element	Fitted value
R_s	662.1 Ω
R_{ct}	46.44 Ω
W	192.2 σ
C_{dl}	6.037 μF

~1330 cm^{-1} due to the graphene structural defects, the second one (G peak) appearing at ~1578 cm^{-1} related to carbon–carbon vibration, and the third one is the 2D harmonic peak localized at ~2660 cm^{-1}.[60] A G-to-D ratio higher than unity indicates significant graphitization of the polyimide film upon laser irradiation.[61] The emergence of an intense 2D peak further confirms its three-dimensional structure and thickness.[61]

3.5. Optimization of the detection parameters

The parameters, affecting the electroanalytical response of the electrodes for Pb^{2+} and Cd^{2+} detection, were also optimized using square-wave anodic stripping voltammetry. These parameters included the deposition potential, deposition time, frequency, and pH of the medium. The optimized voltammograms are shown in Fig. S6,† and the corresponding histograms are shown in Fig. 4. All

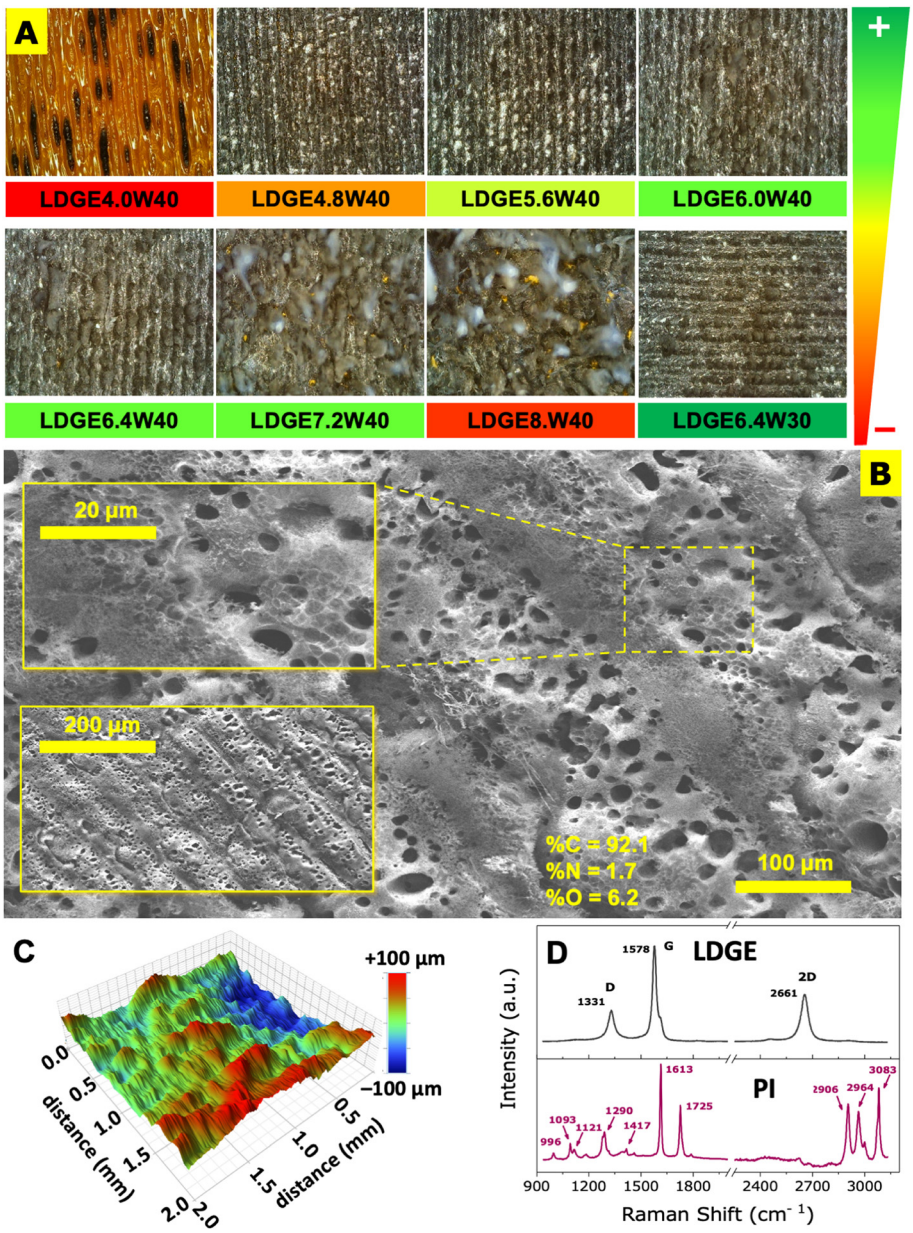

Fig. 3 (A) Digital images of the LDGEs prepared a different sets of laser power and speed; (B) SEM image of LDGE6.4W30 at different magnifications; (C) 3D optical profilometry of LDGE6.4W30; (D) Raman spectra of the polyimide film (blue) and LDGE (black) prepared at a laser power: 6.4 W and laser speed of 30 cm s^{-1}.

Open Access Article. Published on 16 January 2025. Downloaded on 4/26/2026 5:57:25 PM.
This article is licensed under a Creative Commons Attribution-NonCommercial 3.0 Unported Licence.

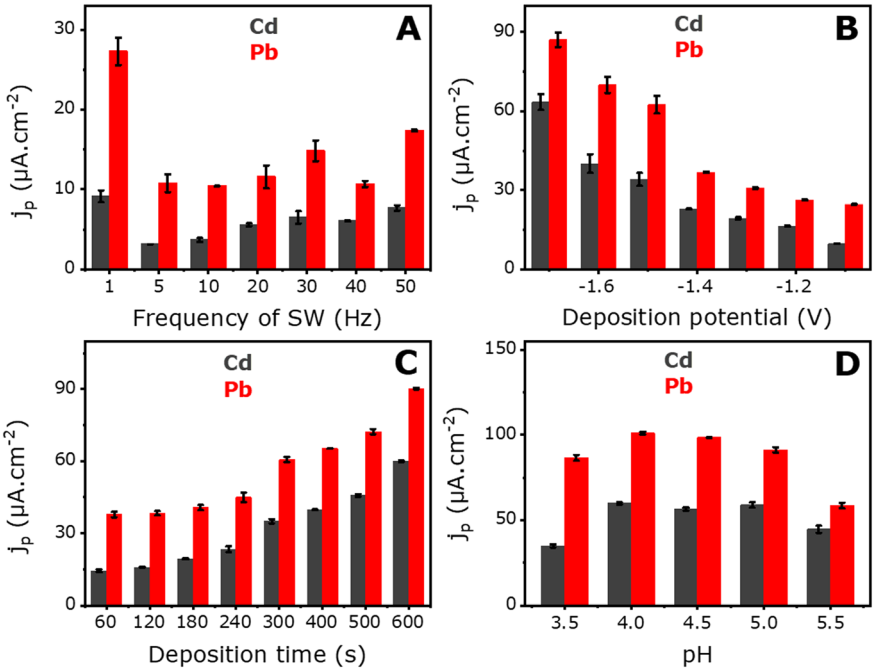

Fig. 4 Histograms of SWASV responses for the optimization of (A) frequency of square wave, (B) deposition potential, (C) deposition time, and (D) medium pH.

experiments were conducted in a 0.1 M acetate-buffered solution at pH 4 containing 250 ppb Pb^{2+} and Cd^{2+}.

3.5.1. Frequency. The frequency was systematically varied between 1 and 50 Hz, keeping other parameters unchanged (deposition potential: −1.3 V, deposition time: 180 s, equilibration time: 30 s). The voltammograms (see ESI†) revealed that the optimal response was obtained at the lowest frequency (1 Hz), while poor responses were observed at higher frequencies. Notably, the signal intensity was three to five times lower at frequencies beyond the optimum (Fig. 4A).

3.5.2. Deposition potential. Subsequently, the effect of the deposition potential was investigated in the potential range of −1.7 to −1.1 V, maintaining a frequency of 1 Hz. The histogram in Fig. 4B shows an improved response as the deposition potential became more cathodic. Therefore, a potential −1.7 V was determined as the optimal deposition potential. This can be explained by the fact that at this potential, there is a strong accumulation of Pb and Cd ions on the surface of the LDGE electrode.

3.5.3. Deposition time. The deposition time was varied from 60 s to 600 s, and the results shown in Fig. 4C show increasing current responses with longer deposition times. However, 180 s was chosen as the deposition time for further electroanalysis because of its ability to yield high sensitivity, excellent resolution in voltammograms, and an overall shortened process time.

3.5.4. Medium pH. Finally, the pH of the acetate-buffered solution was optimized by recording the electrochemical signals for the redissolution of the deposited metallic lead and cadmium at various pH levels (3.5 to 5.5). The histogram in Fig. 4D indicates that the best analytical response was obtained at pH 4. Indeed, the current density increased from pH 3.5 to 4.0 and 4.5 then decreased at higher pH values. The optimal pH value is close to that of the pK_a of the acetic acid/acetate couple. For pH values below 4, there is a competition between H^+ protons and heavy metal ions during the accumulation stage. This reduces the electroanalytical response. Beyond the pK_a value, this effect is diminished, but acidity also decreases. This decreases the electrochemical response.

3.6. Simultaneous detection of cadmium and lead ions

After optimizing the key operational parameters, we examined the simultaneous detection of Pb^{2+} and Cd^{2+} in an acetate-buffered electrolytic solution with varying target ion concentrations. The results showed that the sensor exhibits greater sensitivity to lead compared to cadmium, due to a higher affinity of the LDGE for lead over cadmium.

3.6.1. In spiked solutions. The voltametric responses for lead and cadmium redissolution were recorded at an optimal pH of 4.0. As seen in Fig. 5A, the anodic stripping voltammograms displayed two well-resolved peaks at −0.85 V and −0.59 V corresponding to the oxidation of metallic cadmium and lead, respectively. As shown in Fig. 5B, the peak current densities exhibited a linear increase with the initial concentrations of Cd^{2+} and Pb^{2+} in the solution, ranging widely from 25 to 1000 ppb and 10 to 500 ppb, respectively, for Cd^{2+} and Pb^{2+}. The sensor exhibited sensitivities of 0.161 and 0.333 µA ppb^{-1} cm^{-2} for Cd and Pb, respectively. The calibration curve equations were as follows:

© 2025 The Author(s). Published by the Royal Society of Chemistry

Open Access Article. Published on 16 January 2025. Downloaded on 4/26/2026 5:57:25 PM.
This article is licensed under a Creative Commons Attribution-NonCommercial 3.0 Unported Licence.

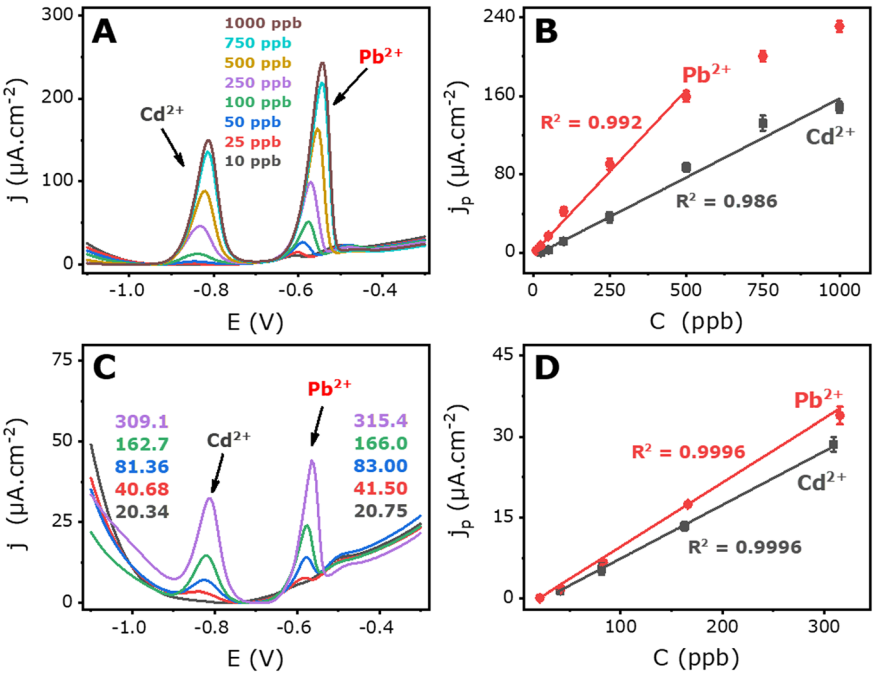

Fig. 5 SWASV responses of cadmium and lead stripping of (A) spiked acetate-buffered solutions and their calibration curve (B) and (C) ore sample solution and its calibration curve (D) using optimal parameters.

$$j_p\ (\mu A\ cm^{-2}) = 0.161 \times [Cd^{2+}]\ (ppb) - 3.530 \quad (R^2 = 0.986) \quad (1)$$

$$j_p\ (\mu A\ cm^{-2}) = 0.333 \times [Pb^{2+}]\ (ppb) - 0.550 \quad (R^2 = 0.991) \quad (2)$$

The detection limits were calculated by dividing 3 times the standard deviation of the blank responses, σ_0 (n = 10), by the slope of the calibration curve. The determined detection limits were 6.13 ppb and 2.96 ppb (at S/N = 3) for Cd^{2+} and Pb^{2+}, respectively. The detection limit obtained for cadmium is comparable to the WHO standard (10 ppb),[62] while that for lead falls below the WFD (5 ppm).[6] The LDGE electrode owes this performance to the heteroatoms such as oxygen and nitrogen present in the material.

During the detection process, electrostatic interactions occurred between the platform and the Cd^{2+} and Pb^{2+} cations, leading to their reduction at the polarized electrode surface to form Cd(0) and Pb(0). Subsequently, after a 30 second equilibration period with the circuit open, a potential scan towards anodic values was performed to oxidize the deposited metals into Cd^{2+} and Pb^{2+}.

The detection mechanism for Pb^{2+} and Cd^{2+} on the surface of the LDGE electrode probably involves mainly the adsorption and stripping steps and one intermediated equilibration step. The first step involves the deposition of metal ions on the electrode surface (M^0_{ads}), while the last one consists of their redissolution into the solution (M^{2+}_{sol}). The different steps can be schematized as follow:

$$\text{Accumulation: LDGE} + M^{2+} \overset{+2e}{\rightarrow} \text{LDGE}\cdots M^0_{ads} \quad (3)$$

Equilibration: circuit is open for 30 seconds

$$\text{Anodic stripping: LDGE}\cdots M^0 \overset{-2e}{\rightarrow} \text{LDGE} + M^{2+}_{sol} \quad (4)$$

3.6.2. In ore samples. To validate the proposed method, the detection of cadmium and lead was assessed in real water samples using aqueous acidic solutions obtained from the dissolution of heavy metal-rich minerals previously determined by atomic absorption spectroscopy. Working solutions were prepared by mixing real samples with an acetate-buffered solution (in equal volumes) and adjusting the pH of the final solution to 4. Five samples with concentrations of (20.34 and 20.75 ppb), (40.68 and 41.5 ppb), (81.36 and 83 ppb), (162.72 and 166 ppb), and (309.10 and 315.4 ppb) of Cd^{2+} and Pb^{2+} were prepared and numbered from 1 to 5.

In Fig. 5C, anodic redissolution voltammograms are displayed, while Fig. 5D shows the peak current densities *vs.* the concentration of both ions. The plots exhibited a linear increase with the increase in Cd^{2+} and Pb^{2+} concentrations, covering ranges of 20.34 to 309.1 ppb and 20.75 to 315.4 ppb for Cd^{2+} and Pb^{2+}, respectively. The electrode exhibited sensitivities of 0.100 and 0.119 µA ppb^{-1} cm^{-2} for Cd and Pb ions, respectively. The calibration curve equations were as follows:

$$j_p\ (\mu A\ cm^{-2}) = 0.100 \times [Cd^{2+}] - 2.578 \quad (R^2 = 0.9996) \quad (5)$$

$$j_p\ (\mu A\ cm^{-2}) = 0.119 \times [Pb^{2+}] - 2.316 \quad (R^2 = 0.9995) \quad (6)$$

These results demonstrate that the LDGE6.4W30 electrode can effectively detect cadmium and lead simultaneously in real samples, such as those from minerals.

Open Access Article. Published on 16 January 2025. Downloaded on 4/26/2026 5:57:25 PM.
This article is licensed under a Creative Commons Attribution-NonCommercial 3.0 Unported Licence.

3.7. Reproducibility, interference and real samples

3.7.1. Reproducibility of the electrode preparation. The reproducibility of the electrode was investigated under optimal conditions in a buffered solution containing 250 ppb Pb^{2+} and Cd^{2+}. Five electrodes were fabricated and activated under the same conditions and subsequently used for the simultaneous detection of the ions. The anodic redissolution voltammograms of the five electrodes are shown in Fig. 6A. As illustrated in the histogram in Fig. 6B, the results demonstrate that the current densities of metal oxidation were very close for the five electrodes, with standard deviations of 1.06% and 0.53% for Cd^{2+} and Pb^{2+}, respectively. This indicates a high level of reproducibility in the analysis from one electrode to another, indicating consistent and reliable performance across multiple electrode fabrication processes.

3.7.2. Interference. The interference of other metallic cations, including Zn^{2+}, Cu^{2+}, Co^{2+}, and Ba^{2+}, on the electrochemical analysis of Pb^{2+} and Cd^{2+} was systemically examined. Initially, a voltammogram for a solution containing 250 ppb Pb^{2+} and 250 ppb Cd^{2+} alone was recorded and set as the reference, labeled as "Ref." in Fig. 6C.

Subsequently, various concentrations of interfering cations (*i.e.*, 500, 1000, and 1500 ppb) were introduced into the former solution before recording their voltammograms (red, blue, green, and purple curves in Fig. 6C). The superimposed voltammograms illustrate that the signals for Zn^{2+}, Co^{2+}, and Cu^{2+} appear at potentials different from those of Cd^{2+} and Pb^{2+}, enabling the simultaneous detection of Pb^{2+} and Cd^{2+}, even in the presence of other ions. Notably, this capability was extended to concentrations six times higher than those of the target cations (Table S1†). We observe a significant shift in the anodic peak potential of cadmium and lead after addition of the concentration of interfering ions. This effect can be explained probably by the interfering ions like Ba^{2+} who react with the metallic film to delay oxidation step of Cd^{2+} and Pb^{2+} during stripping process.

3.7.3. Detection in real samples. Considering the past use of lead-containing alloys in pipe fabrication in Tunisia, tap water was used to determine the presence of Pb^{2+} ions. The two electrodes were fabricated under the same conditions for the assay, and the voltammograms of both electrodes are shown in Fig. 6D.

The results indicated that the peak current densities for the oxidation of Pb^{2+} and Cd^{2+} were of the same magnitude as the initial concentrations of the target ions. This finding signifies the absence of Pb^{2+} in tap water, suggesting that the water sampled from the tap did not contain detectable levels of lead ions. This observation is crucial for assessing the safety of tap water, especially in regions where lead-containing materials have historically been used in water infrastructure.

Discussion

Over the years, the production of commercial sensors for the analysis and detection of heavy metal ions in water bodies has become prevalent. An effective sensor is characterized by simplicity in manufacturing and cost of materials, which

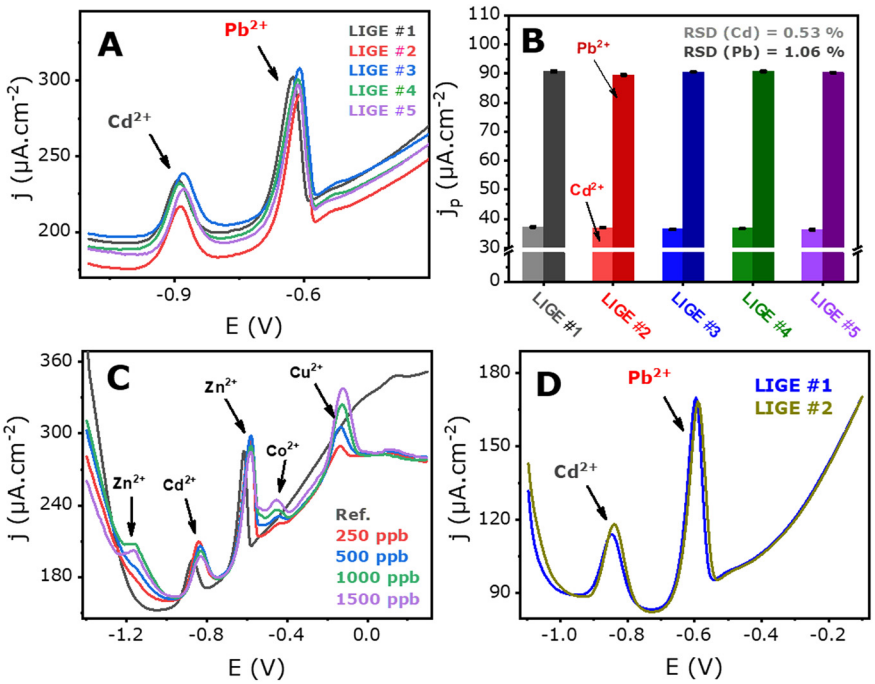

Fig. 6 (A) SWASV response reproducibility for five electrodes prepared using the same laser writing conditions; (B) current density histograms showing the weak RSD; (C) SWASV responses of 250 ppb of Cd^{2+} and Pb^{2+} with interfering metallic ions at 250, 500, 1000 and 1500 ppb and (D) SWASV responses for two different electrodes tested in tap water.

© 2025 The Author(s). Published by the Royal Society of Chemistry

Open Access Article. Published on 16 January 2025. Downloaded on 4/26/2026 5:57:25 PM. This article is licensed under a Creative Commons Attribution-NonCommercial 3.0 Unported Licence.

directly influences the overall market cost. Simplicity in sensor usage and short electroanalysis time are vital quality characteristics that are essential for designing an ideal sensor that is accessible to a wide range of users.

Laser-derived graphene electrodes have garnered significant attention over the past decade owing to their straightforward fabrication process, which eliminates the need for chemical or complex chemical processes. Typically, a PET sheet, polyimide film adhesive tape, and affordable laser cutting/engraving device are the primary components required to carbonize the PI film and generate graphene. The simplicity of this method contributes to the appeal of this process for sensor applications. However, it is worth noting that some researchers applied precursors to the surface before laser treatment, resulting in modified LDGEs with composite compositions influenced by the precursors used.[63]

The developed LDGE6.4W30 electrode, employed in an aqueous environment, demonstrated efficient detection of target cations over a wide range of concentrations (25–1000 ppb for Cd^{2+} and 10–500 ppb for Pb^{2+}). The detection limits were found to be 6.13 and 2.96 ppb, with sensitivities of 0.161 and 0.333 μA ppb^{-1} cm^{-2}, respectively, for Cd^{2+} and Pb^{2+}. These performances are notably satisfactory compared to many other laser-derived graphene-based sensors described in recent literature, many of which have manufacturing processes[64,65] that provide results comparable to those of unmodified LDGEs, which are obtained by fine-tuning the laser power and speed and minimal pretreatment (refer to Table 2).

Porous LDGEs have a more conductive structure than laser-derived graphene fiber (LIGF) electrodes.[32] Jeong *et al.*[55] developed an electrochemical sensor based on LIGF as the working electrode; a bismuth film was electrodeposited *in situ* on the LIGF surface for electrochemical detection of cadmium and lead ions. The LIGF-based heavy metal sensor has low detection limits of 0.4 μg L^{-1} for Cd and Pb ions. This detection limit is lower than that in our study. Perhaps in terms of conduction, porous structures are better, as stipulated by Abdulhafez *et al.* Nevertheless, this electrode preparation method is very simple, does not require a long preparation time, and results in exceptional performance.

The LDGE6.4W30 electrode displayed a higher detection limit than some other LDGE-based electrodes,[64,65] which is attributed to the rigorous optimization process. The electrochemical sensor efficiency for detecting Cd^{2+} and Pb^{2+} can be attributed to the porosity of the laser-derived electrode, which enhances the active surface area owing to the 3D structure of the produced graphene. This 3D porous structure allows metal ions to be incorporated during the accumulation step, with potential difficulties during the reoxidation of the initially reduced metals, especially during rapid scanning. Consequently, the responses were suboptimal and exhibited larger oxidation peaks at high frequencies (or scan rates), but improved at low frequencies, particularly at 1 Hz. In the latter case, the SWASV responses exhibited distinct and fine oxidation peaks for cadmium and lead.

In environmental analysis, the sensor showed exceptional performance for both tap water and mineral water samples. Even in this complex matrix of tap water, the sensor efficiently achieved the simultaneous detection of Cd^{2+} and Pb^{2+} with well-defined peaks, highlighting its electrochemical stability and selectivity. Repetitive measurements demonstrated close current densities of the recorded voltammogram peaks, emphasizing platform stability in the detection of heavy metal ions in challenging matrices.

Successful detection of Pb^{2+} and Cd^{2+} ions was also demonstrated in aqueous solutions prepared from dissolving minerals, with Pb^{2+} and Cd^{2+} contents determined by atomic absorption spectroscopy. The sensor proved its efficiency in the simultaneous detection of target ions in this complex matrix, with well-defined peaks nearly overlapping the average of three repetitive measurements of the targeted ions. This underscores not only the electrochemical stability and selectivity, but also the capability of the sensor to simultaneously detect Cd^{2+} and Pb^{2+} ions in such intricate environmental samples.

Conclusion

This analysis effectively showed the efficient production of highly cost-effective laser-derived graphene 3D porous

Table 2 Comparison of different LDGE for the detection of Cd^{2+} and Pb^{2+}

Electrodes[a]	Technique	Linear range (ppb)		LOD (ppb)		Real sample	Ref.
		Cd^{2+}	Pb^{2+}	Cd^{2+}	Pb^{2+}		
LIGF	SWASV	1.0–140.0	1.0–140.0	0.4	0.4	Drinking water and tap water	55
AgNPs/LIG	SWASV	0.0–120	0.0–120	0.1	0.1	Tap water and drinking water	56
SnO_2/CeO_2/LIG	DPASV	0.1–160	—	0.01	—	Groundwater and tap water	57
Nafion/BiNPs@LIG	SWASV	5–50	5–50	0.5	0.8	NT[b]	63
LICE	DPASV	—	50–350	—	33	NT[b]	64
N@LEG/GCE	SWASV	5–10, 10–380	0.5–10, 10–380	1.08	0.16	Lake water	66
IL/PLC/LEGE	SWASV	—	1–80	—	0.17	Tap water and lake water	67
LEGCNs	SWASV	7–120	5–120	0.47	0.41	Real water samples	68
LDGE6.4W30	SWASV	25–1000	10–500	6.13	2.93	Acid-dissolved ores	This work

[a] LIGF: laser-derived graphene fiber; LIG: laser-induced graphene; AgNPs: silver nanoparticles; BiNPs: bismuth nanoparticles; LICE: laser-induced carbon electrode; N@LEG: nitrogen-doped laser engraved graphene; IL: ionic liquid; PLC: poly-L-cysteine; LEGE: laser-engraved graphene electrode; LEGCNs: laser etched graphene-based carbon nanomaterials. [b] Not tested.

Open Access Article. Published on 16 January 2025. Downloaded on 4/26/2026 5:57:25 PM. This article is licensed under a Creative Commons Attribution-NonCommercial 3.0 Unported Licence.

electrodes for the detection of heavy metal ions without any further treatment or nanostructuration with nanomaterials. By modifying the laser writing parameters, the performance of the electrode was considerably improved, thereby eliminating the need for additional nanomaterials. The resulting sensor was used to measure Cd^{2+} and Pb^{2+} in spiked acetate-buffered solutions, exhibiting a linear response in the concentration range of 25–1000 ppb (with a LOD of 6.13 ppb) for Cd^{2+} and 10–500 ppb (with a LOD of 2.96 ppb) for Pb^{2+}. Additionally, the electrochemical sensor demonstrated its ability to simultaneously detect both ions in real samples, such as ore and tap water, with minimal matrix interference. The ease of fabrication and versatility of the sensor makes it easily producible, making it a suitable option for detecting heavy metal ions in drinking water, particularly in low-resource settings. This highlights the potential for practical applications, where simplicity, efficiency, and cost-effectiveness are essential considerations. Our work will open up promising prospects for the application of composite-modified LDGE, both before and/or after laser scribing, to enable more sensitive detection of heavy metal ions and other pollutants.

Abbreviations

A	Surface area
ABS	Acetate-buffered solution
ASV	Anodic stripping voltammetry
CNT(s)	Carbon nanotube(s)
CV	Cyclic voltammetry
D	Diffusion coefficient
DI	deionized water
DPASV	Differential pulse anodic stripping voltammetry
EDX	Energy-dispersive X-ray spectroscopy
EIS	Electrochemical impedance spectroscopy
EPA	US Environmental Protection Agency
F_{SW}	Frequency of square wave
FDA	US Food and Drug Administration
LDGE	Laser-derived graphene electrode
LIGF	Laser-induced graphene fiber
LOD	Limit of detection
LOQ	Limit of quantification
PET	Polyethylene terephthalate
pH	Potential of hydrogen
PI	Polyimide
pK_a	Acid dissociation constant
R_{ct}	Charge-transfer resistance
SEM	Scanning electron microscopy
SWASV	Square wave anodic stripping voltammetry
WFD	EU Water Framework Directive
WHO	World Health Organization

Data availability

The data underlying this study are available in the published article and its ESI.†

Author contributions

I. D.: writing – review & editing, investigation, formal analysis, data curation; A. R.: formal analysis, data curation, investigation; M. F.: writing – review & editing, formal analysis; S. H.: writing – review & editing; N. R.: writing – review & editing, supervision, resources, conceptualization.

Conflicts of interest

The authors declare that they have no known competing financial interests or personal relationships that could have appeared to influence the work reported in this paper.

Acknowledgements

No funding was received for conducting this study. I. D. thanks the International Science Program (ISP) from the Uppsala University (Uppsala, Sweden) for the mobility support through the ANEC network.

References

1 S. Goudarzi, S. A. Jozi, S. M. Monavari, A. Karbasi and A. H. Hasani, Assessment of Groundwater Vulnerability to Nitrate Pollution Caused by Agricultural Practices, *Water Qual. Res. J.*, 2017, **52**(1), 64–77, DOI: **10.2166/wqrjc.2017.031**.

2 P. J. Sajil Kumar, P. Jegathambal and E. J. James, Chemometric Evaluation of Nitrate Contamination in the Groundwater of a Hard Rock Area in Dharapuram, South India, *Appl. Water Sci.*, 2014, **4**(4), 397–405, DOI: **10.1007/s13201-014-0155-0**.

3 S. Mukherjee, S. Bhattacharyya, K. Ghosh, S. Pal, A. Halder, M. Naseri, M. Mohammadniaei, S. Sarkar, A. Ghosh, Y. Sun and N. Bhattacharyya, Sensory Development for Heavy Metal Detection: A Review on Translation from Conventional Analysis to Field-Portable Sensor, *Trends Food Sci. Technol.*, 2021, **109**, 674–689, DOI: **10.1016/j.tifs.2021.01.062**.

4 I. Diédhiou, B. Fall, C. Gaye, M. L. Sall, A. K. D. Diaw, D. Gningue-Sall, M. Fall and N. Raouafi, Preparations and Applications of Organic Conducting Polymers/Graphene Composites in Heavy Metal Ion Sensing: A Review, *Int. J. Mater. Res.*, 2023, **114**(2), 79–99, DOI: **10.1515/ijmr-2021-8596**.

5 S. Mitra, A. J. Chakraborty, A. M. Tareq, T. Bin Emran, F. Nainu, A. Khusro, A. M. Idris, M. U. Khandaker, H. Osman, F. A. Alhumaydhi and J. Simal-Gandara, Impact of heavy metals on the environment and human health: Novel therapeutic insights to counter the toxicity, *J. King Saud Univ., Sci.*, 2022, **34**(3), 101865, DOI: **10.1016/j.jksus.2022.101865**.

6 A. Garciá-Miranda Ferrari, P. Carrington, S. J. Rowley-Neale and C. E. Banks, Recent Advances in Portable Heavy Metal Electrochemical Sensing Platforms, *Environ. Sci.:Water Res. Technol.*, 2020, **6**, 2676–2690, DOI: **10.1039/d0ew00407c**.

7 Y. He, L. Ma, L. Zhou, G. Liu, Y. Jiang and J. Gao, Preparation and Application of Bismuth/MXene Nano-Composite as Electrochemical Sensor for Heavy Metal Ions Detection, *Nanomaterials*, 2020, **10**(5), 866, DOI: **10.3390/nano10050866**.

© 2025 The Author(s). Published by the Royal Society of Chemistry

Open Access Article. Published on 16 January 2025. Downloaded on 4/26/2026 5:57:25 PM. This article is licensed under a Creative Commons Attribution-NonCommercial 3.0 Unported Licence.

8 L. Nejdl, J. Kudr, K. Cihalova, D. Chudobova, M. Zurek, L. Zalud, L. Kopecny, F. Burian, B. Ruttkay-Nedecky, S. Krizkova, M. Konecna, D. Hynek, P. Kopel, J. Prasek, V. Adam and R. Kizek, Remote-Controlled Robotic Platform ORPHEUS as a New Tool for Detection of Bacteria in the Environment, *Electrophoresis*, 2014, **35**(16), 2333–2345, DOI: **10.1002/elps.201300576**.

9 A. M. de Campos, R. R. Silva, M. L. Calegaro and P. A. Raymundo-Pereira, Design and Fabrication of Flexible Copper Sensor Decorated with Bismuth Micro/Nanodentrites to Detect Lead and Cadmium in Noninvasive Samples of Sweat, *Chemosensors*, 2022, **10**(11), 446, DOI: **10.3390/chemosensors10110446**.

10 R. R. Silva, P. A. Raymundo-Pereira, A. M. Campos, D. Wilson, C. G. Otoni, H. S. Barud, C. A. R. Costa, R. R. Domeneguetti, D. T. Balogh, S. J. L. Ribeiro and O. N. Oliveira Jr., Microbial Nanocellulose Adherent to Human Skin Used in Electrochemical Sensors to Detect Metal Ions and Biomarkers in Sweat, *Talanta*, 2020, **218**, 121153, DOI: **10.1016/j.talanta.2020.121153**.

11 M. Lo, M. Seydou, A. Bensghaïer, R. Pires, D. Gningue-Sall, J. J. Aaron, Z. Mekhalif, J. Delhalle and M. M. Chehimi, Polypyrrole-Wrapped Carbon Nanotube Composite Films Coated on Diazonium-Modified Flexible ITO Sheets for the Electroanalysis of Heavy Metal Ions, *Sensors*, 2020, **20**(3), 580, DOI: **10.3390/S20030580**.

12 S. M. Seck, S. Charvet, M. Fall, E. Baudrin, F. Geneste, M. Lejeune and M. Benlahsen, Functionalization of Amorphous Nitrogenated Carbon Thin Film Electrodes for Improved Detection of Cadmium vs. Copper Cations, *J. Electroanal. Chem.*, 2015, **738**, 154–161, DOI: **10.1016/J.JELECHEM.2014.11.013**.

13 G. Aragay and A. Merkoçi, Nanomaterials Application in Electrochemical Detection of Heavy Metals, *Electrochim. Acta*, 2012, **84**, 49–61, DOI: **10.1016/j.electacta.2012.04.044**.

14 L. Pujol, D. Evrard, K. Groenen-Serrano, M. Freyssinier, A. Ruffien-Cizsak and P. Gros, Electrochemical Sensors and Devices for Heavy Metals Assay in Water: The French Groups' Contribution, *Front. Chem.*, 2014, **2**, DOI: **10.3389/fchem.2014.00019**.

15 H. N. Nayan Kumar, D. H. Nagaraju, Z. Yhobu, P. Shivakumar, K. S. Manjunatha Kumara, S. Budagumpi and B. M. Praveen, Recent Advances in On-Site Monitoring of Heavy Metal Ions in the Environment, *Microchem. J.*, 2022, **182**, 107894, DOI: **10.1016/j.microc.2022.107894**.

16 Y. Qiao, Q. Liu, S. Lu, G. Chen, S. Gao, W. Lu and X. Sun, High-Performance Non-Enzymatic Glucose Detection: Using a Conductive Ni-MOF as an Electrocatalyst, *J. Mater. Chem. B*, 2020, **8**(25), 5411–5415, DOI: **10.1039/D0TB00131G**.

17 M. Wei, Y. Qiao, H. Zhao, J. Liang, T. Li, Y. Luo, S. Lu, X. Shi, W. Lu and X. Sun, Electrochemical Non-Enzymatic Glucose Sensors: Recent Progress and Perspectives, *Chem. Commun.*, 2020, **56**(93), 14553–14569, DOI: **10.1039/D0CC05650B**.

18 N. O. Gomes, R. T. Paschoalin, S. Bilatto, A. R. Sorigotti, C. S. Farinas, L. H. C. Mattoso, S. A. S. Machado, O. N. Oliveira Jr and P. A. Raymundo-Pereira, Flexible, Bifunctional Sensing Platform Made with Biodegradable Mats for Detecting Glucose in Urine, *ACS Sustainable Chem. Eng.*, 2023, **11**(6), 2209–2218, DOI: **10.1021/acssuschemeng.2c05438**.

19 S. Ben Aissa, M. Mastouri, G. Catanante, N. Raouafi and J. L. Marty, Investigation of a Truncated Aptamer for Ofloxacin Detection Using a Rapid FRET-Based Apta-Assay, *Antibiotics*, 2020, **9**(12), 860, DOI: **10.3390/antibiotics9120860**.

20 M. Hamami, M. Bouaziz, N. Raouafi, A. Bendounan and H. Korri-Youssoufi, MoS2/PPy Nanocomposite as a Transducer for Electrochemical Aptasensor of Ampicillin in River Water, *Biosensors*, 2021, **11**(9), 311, DOI: **10.3390/bios11090311**.

21 P. A. Raymundo-Pereira, N. O. Gomes, F. M. Shimizu, S. A. S. Machado and O. N. Oliveira, Selective and Sensitive Multiplexed Detection of Pesticides in Food Samples Using Wearable, Flexible Glove-Embedded Non-Enzymatic Sensors, *Chem. Eng. J.*, 2021, **408**, 127279, DOI: **10.1016/j.cej.2020.127279**.

22 R. T. Paschoalin, N. O. Gomes, G. F. Almeida, S. Bilatto, C. S. Farinas, S. A. S. Machado, L. H. C. Mattoso, O. N. Oliveira and P. A. Raymundo-Pereira, Wearable Sensors Made with Solution-Blow Spinning Poly(Lactic Acid) for Non-Enzymatic Pesticide Detection in Agriculture and Food Safety, *Biosens. Bioelectron.*, 2022, **199**, 113875, DOI: **10.1016/j.bios.2021.113875**.

23 N. Oezau Gomes, A. M. de Campos, M. L. Calegaro, S. A. S. Machado, O. N. Oliveira Jr. and P. A. Raymundo-Pereira, Core–Shell Nanocables Decorated with Carbon Spherical Shells and Silver Nanoparticles for Sensing Ethinylestradiol Hormone in Water Sources and Pills, *ACS Appl. Mater. Interfaces*, 2024, **16**(8), 10897–10907, DOI: **10.1021/acsami.3c16249**.

24 N. O. Gomes and P. A. Raymundo-Pereira, On-Site Therapeutic Drug Monitoring of Paracetamol Analgesic in Non-Invasively Collected Saliva for Personalized Medicine, *Small*, 2023, **19**(12), 2206753, DOI: **10.1002/smll.202206753**.

25 X. Chen, F. Luo, M. Yuan, D. Xie, L. Shen, K. Zheng, Z. Wang, X. Li and L. Tao, A Dual-Functional Graphene-Based Self-Alarm Health-Monitoring E-Skin, *Adv. Funct. Mater.*, 2019, **29**(51), 1904706, DOI: **10.1002/adfm.201904706**.

26 J. B. In, B. Hsia, J.-H. Yoo, S. Hyun, C. Carraro, R. Maboudian and C. P. Grigoropoulos, Facile Fabrication of Flexible All Solid-State Micro-Supercapacitor by Direct Laser Writing of Porous Carbon in Polyimide, *Carbon*, 2015, **83**, 144–151, DOI: **10.1016/j.carbon.2014.11.017**.

27 L. Li, J. Zhang, Z. Peng, Y. Li, C. Gao, Y. Ji, R. Ye, N. D. Kim, Q. Zhong, Y. Yang, H. Fei, G. Ruan and J. M. Tour, High-Performance Pseudocapacitive Microsupercapacitors from Laser-Induced Graphene, *Adv. Mater.*, 2016, **28**(5), 838–845, DOI: **10.1002/adma.201503333**.

28 S. P. Singh, Y. Li, A. Be'er, Y. Oren, J. M. Tour and C. J. Arnusch, Laser-Induced Graphene Layers and Electrodes Prevents Microbial Fouling and Exerts Antimicrobial Action, *ACS Appl. Mater. Interfaces*, 2017, **9**(21), 18238–18247, DOI: **10.1021/acsami.7b04863**.

29 M. G. Stanford, C. Zhang, J. D. Fowlkes, A. Hoffman, I. N. Ivanov, P. D. Rack and J. M. Tour, High-Resolution Laser-

Open Access Article. Published on 16 January 2025. Downloaded on 4/26/2026 5:57:25 PM. This article is licensed under a Creative Commons Attribution-NonCommercial 3.0 Unported Licence.

Induced Graphene. Flexible Electronics beyond the Visible Limit, *ACS Appl. Mater. Interfaces*, 2020, **12**(9), 10902–10907, DOI: **10.1021/acsami.0c01377**.

30 Q. Huang and Y. Zhu, Printing Conductive Nanomaterials for Flexible and Stretchable Electronics: A Review of Materials, Processes, and Applications, *Adv. Mater. Technol.*, 2019, **4**(5), 1800546, DOI: **10.1002/admt.201800546**.

31 D. S. Saidina, N. Eawwiboonthanakit, M. Mariatti, S. Fontana and C. Hérold, Recent Development of Graphene-Based Ink and Other Conductive Material-Based Inks for Flexible Electronics, *J. Electron. Mater.*, 2019, **48**(6), 3428–3450, DOI: **10.1007/s11664-019-07183-w**.

32 M. Abdulhafez, G. N. Tomaraei and M. Bedewy, Fluence-Dependent Morphological Transitions in Laser-Induced Graphene Electrodes on Polyimide Substrates for Flexible Devices, *ACS Appl. Nano Mater.*, 2021, **4**(3), 2973–2986, DOI: **10.1021/acsanm.1c00101**.

33 R. Rahimi, M. Ochoa, W. Yu and B. Ziaie, Highly Stretchable and Sensitive Unidirectional Strain Sensor via Laser Carbonization, *ACS Appl. Mater. Interfaces*, 2015, **7**(8), 4463–4470, DOI: **10.1021/am509087u**.

34 A. A. Lahcen, S. Rauf, T. Beduk, C. Durmus, A. Aljedaibi, S. Timur, H. N. Alshareef, A. Amine, O. S. Wolfbeis and K. N. Salama, Electrochemical Sensors and Biosensors Using Laser-Derived Graphene: A Comprehensive Review, *Biosens. Bioelectron.*, 2020, **168**, 112565, DOI: **10.1016/j.bios.2020.112565**.

35 A. Rabti, S. Baachaoui, O. Ghodbane and N. Raouafi, Laser-ablated graphene electrodes modified with redox melanin-like film for redox capacitive sensing via the scavenging of nitrite ions, *Food Chem.*, 2024, **469**, 142509, DOI: **10.1016/j.foodchem.2024.142509**.

36 B. Ouedraogo, S. Baachaoui, A. Tall, I. Tapsoba and N. Raouafi, Laser-Induced Graphene Electrodes on Polyimide Membranes Modified with Gold Nanoparticles for the Simultaneous Detection of Dopamine and Uric Acid in Human Serum, *Microchim. Acta*, 2023, **190**(8), 316, DOI: **10.1007/s00604-023-05909-6**.

37 A. Berni, A. Ait Lahcen, K. N. Salama and A. Amine, 3D-Porous Laser-Scribed Graphene Decorated with Overoxidized Polypyrrole as an Electrochemical Sensing Platform for Dopamine, *J. Electroanal. Chem.*, 2022, **919**, 116529, DOI: **10.1016/j.jelechem.2022.116529**.

38 S. Baachaoui, W. Mabrouk, K. Charradi, B. Slimi, A. M. Ramadan, R. M. I. Elsamra, A. Alhussein, S. M. A. S. Keshk and N. Raouafi, Laser-Induced Porous Graphene Electrodes from Polyketimine Membranes for Paracetamol Sensing, *R. Soc. Open Sci.*, 2023, **10**(8), 230294, DOI: **10.1098/rsos.230294**.

39 A. Raouafi, I. Diedhiou, A. H. Almarri and N. Raouafi, Gold-Modified Laser-Scribed Lettuce-like Graphene Electrodes for Ultrasensitive Detection of Bioactive Molecules, *Emergent Mater.*, 2024, **7**(6), 2945–2955, DOI: **10.1007/s42247-024-00750-w**.

40 A. Ghanam, A. A. Lahcen, T. Beduk, H. N. Alshareef, A. Amine and K. N. Salama, Laser Scribed Graphene: A Novel Platform for Highly Sensitive Detection of Electroactive Biomolecules, *Biosens. Bioelectron.*, 2020, **168**, 112509, DOI: **10.1016/j.bios.2020.112509**.

41 A. Berni, A. A. Lahcen and A. Amine, Electrochemical Sensing of Paracetamol Using 3D Porous Laser Scribed Graphene Platform, *Electroanalysis*, 2023, **35**(4), e202200137, DOI: **10.1002/elan.202200137**.

42 A. Berni, A. Amine, J. J. García-Guzmán, L. Cubillana-Aguilera and J. M. Palacios-Santander, Feather-like Gold Nanostructures Anchored onto 3D Mesoporous Laser-Scribed Graphene: A Highly Sensitive Platform for Enzymeless Glucose Electrochemical Detection in Neutral Media, *Biosensors*, 2023, **13**(7), 678, DOI: **10.3390/bios13070678**.

43 A. C. Marques, A. R. Cardoso, R. Martins, M. G. F. Sales and E. Fortunato, Laser-Induced Graphene-Based Platforms for Dual Biorecognition of Molecules, *ACS Appl. Nano Mater.*, 2020, **3**(3), 2795–2803, DOI: **10.1021/acsanm.0c00117**.

44 M. G. Stanford, K. Yang, Y. Chyan, C. Kittrell and J. M. Tour, Laser-Induced Graphene for Flexible and Embeddable Gas Sensors, *ACS Nano*, 2019, **13**(3), 3474–3482, DOI: **10.1021/acsnano.8b09622**.

45 S. Baachaoui, W. Mabrouk, A. Rabti, O. Ghodbane and N. Raouafi, Laser-Induced Graphene Electrodes Scribed onto Novel Carbon Black-Doped Polyethersulfone Membranes for Flexible High-Performance Microsupercapacitors, *J. Colloid Interface Sci.*, 2023, **646**, 1–10, DOI: **10.1016/j.jcis.2023.05.024**.

46 S. Baachaoui, W. Mabrouk, O. Ghodbane and N. Raouafi, Enhancing Energy Storage Performance in Flexible All-Solid-State Laser-Induced Graphene-Based Microsupercapacitors through the Addition of Carbon Black and Prussian Blue, *J. Energy Storage*, 2024, **75**, 109580, DOI: **10.1016/j.est.2023.109580**.

47 I. Diédhiou, A. Sebei, M. Fall, S. B. Aoun, R. Zarrougui and N. Raouafi, Simultaneous Detection of Trace Pb(II) and Cd(II) Cations in Ore Samples by Anodic Stripping Analysis Using pMO/erGO-modified Glassy Carbon Electrodes, *Electroanalysis*, 2023, **35**(12), e202300072, DOI: **10.1002/elan.202300072**.

48 A. Diarisso, M. Fall and N. Raouafi, Elaboration of a Chemical Sensor Based on Polyaniline and Sulfanilic Acid Diazonium Salt for Highly Sensitive Detection Nitrite Ions in Acidified Aqueous Media, *Environ. Sci.: Water Res. Technol.*, 2018, **4**(7), 1024–1034, DOI: **10.1039/C8EW00139A**.

49 V. Suvina, S. M. Krishna, D. H. Nagaraju, J. S. Melo and R. G. Balakrishna, Polypyrrole-Reduced Graphene Oxide Nanocomposite Hydrogels: A Promising Electrode Material for the Simultaneous Detection of Multiple Heavy Metal Ions, *Mater. Lett.*, 2018, **232**, 209–212, DOI: **10.1016/J.MATLET.2018.08.096**.

50 K. S. M. Kumara, P. Shivakumar, V. Ganesh, S. Budagumpi, S. K. Bose, K. Hareesh and D. H. Nagaraju, Hydrogels of PANI Doped with Fe3O4 and GO for Highly Stable Sensor for Sensitive and Selective Determination of Heavy Metal Ions, *Inorg. Chem. Commun.*, 2023, **158**, 111553, DOI: **10.1016/j.inoche.2023.111553**.

51 D. S. Manjunatha Kumara, D. H. Nagaraju, Z. Yhobu, H. N. Nayan Kumar, S. Budagumpi, S. Kumar Bose, P. Shivakumar and V. N. Palakollu, Tuning the Surface Functionality of Fe3O4 for Sensitive and Selective Detection of Heavy Metal Ions, *Sensors*, 2022, **22**(22), 8895, DOI: **10.3390/s22228895**.

© 2025 The Author(s). Published by the Royal Society of Chemistry

Open Access Article. Published on 16 January 2025. Downloaded on 4/26/2026 5:57:25 PM. This article is licensed under a Creative Commons Attribution-NonCommercial 3.0 Unported Licence.

52 T. AL-Gahouari, P. Sayyad, G. Bodkhe, N. Ingle, M. Mahadik, S. Shirsat and M. Shirsat, Controlling Reduction Degree of Graphene Oxide-Based Electrode for Improving the Sensing Performance toward Heavy Metal Ions, *Appl. Phys. A: Mater. Sci. Process.*, 2021, **127**(3), 170, DOI: **10.1007/s00339-020-04199-6**.

53 A. R. Thiruppathi, B. Sidhureddy, W. Keeler and A. Chen, Facile One-Pot Synthesis of Fluorinated Graphene Oxide for Electrochemical Sensing of Heavy Metal Ions, *Electrochem. Commun.*, 2017, **76**, 42–46, DOI: **10.1016/J.ELECOM.2017.01.015**.

54 X. Liu, X. Wang, J. Li, M. Qu, M. Kang and C. Zhang, Nonmodified Laser-Induced Graphene Sensors for Lead-Ion Detection, *ACS Appl. Nano Mater.*, 2023, **6**(5), 3599–3607, DOI: **10.1021/acsanm.2c05307**.

55 S.-E. Jeong, S. Kim, J.-H. Han and J. J. Pak, Simple Laser-Induced Graphene Fiber Electrode Fabrication for High-Performance Heavy-Metal Sensing, *Microchem. J.*, 2022, **172**, 106950, DOI: **10.1016/j.microc.2021.106950**.

56 S. Jeong, S. Yang, Y. J. Lee and S. H. Lee, Laser-Induced Graphene Incorporated with Silver Nanoparticles Applied for Heavy Metal Multi-Detection, *J. Mater. Chem. A*, 2023, **11**(25), 13409–13418, DOI: **10.1039/D3TA00691C**.

57 Y. Liu, Q. Xue, C. Chang, R. Wang, Q. Wang and X. Shan, Highly Efficient Detection of Cd(II) Ions by a Stannum and Cerium Bimetal-Modified Laser-Induced Graphene Electrode in Water, *Chem. Eng. J.*, 2022, **433**, 133791, DOI: **10.1016/j.cej.2021.133791**.

58 B. Fall, A. K. D. Diaw, M. Fall, M. L. Sall, M. Lo, D. Gningue-Sall, M. O. Thotiyl, H. J. Maria, N. Kalarikkal and S. Thomas, Synthesis of Highly Sensitive rGO@CNT@Fe2O3/Polypyrrole Nanocomposite for the Electrochemical Detection of Pb2+, *Mater. Today Commun.*, 2021, **26**, 102005, DOI: **10.1016/J.MTCOMM.2020.102005**.

59 A. Moutcine, C. Laghlimi, O. Ifguis, M. A. Smaini, S. E. El Qouatli, M. Hammi and A. Chtaini, A Novel Carbon Paste Electrode Modified by NP-Al2O3 for the Electrochemical Simultaneous Detection of Pb(II) and Hg(II), *Diamond Relat. Mater.*, 2020, **104**, 107747, DOI: **10.1016/j.diamond.2020.107747**.

60 K. Sangeetha Selvan and S. Sriman Narayanan, Synthesis, Structural Characterization and Electrochemical Studies Switching of MWCNT/Novel Tetradentate Ligand Forming Metal Complexes on PIGE Modified Electrode by Using SWASV, *Mater. Sci. Eng., C*, 2019, **98**, 657–665, DOI: **10.1016/J.MSEC.2018.12.094**.

61 H. Wahab, V. Jain, A. S. Tyrrell, M. A. Seas, L. Kotthoff and P. A. Johnson, Machine-Learning-Assisted Fabrication: Bayesian Optimization of Laser-Induced Graphene Patterning Using in-Situ Raman Analysis, *Carbon*, 2020, **167**, 609–619, DOI: **10.1016/j.carbon.2020.05.087**.

62 A. A. Mohammadi, A. Zarei, S. Majidi, A. Ghaderpoury, Y. Hashempour, M. H. Saghi, A. Alinejad, M. Yousefi, N. Hosseingholizadeh and M. Ghaderpoori, Carcinogenic and Non-Carcinogenic Health Risk Assessment of Heavy Metals in Drinking Water of Khorramabad, Iran, *MethodsX*, 2019, **6**, 1642–1651, DOI: **10.1016/j.mex.2019.07.017**.

63 G. Zhao, X. Wang, G. Liu and N. Thi Dieu Thuy, A Disposable and Flexible Electrochemical Sensor for the Sensitive Detection of Heavy Metals Based on a One-Step Laser-Induced Surface Modification: A New Strategy for the Batch Fabrication of Sensors, *Sens. Actuators, B*, 2022, **350**, 130834, DOI: **10.1016/j.snb.2021.130834**.

64 B. Ding, Q. Zhang, C. Yang, W. Yang, J. Liu, C. Li and S. Tao, Laser-Induced Carbon Electrodes in a Three-Dimensionally Printed Flow Reactor for Detecting Lead Ions, *ACS Omega*, 2021, **6**(19), 12470–12479, DOI: **10.1021/acsomega.0c06274**.

65 B. A. Getachew, D. S. Bergsman and J. C. Grossman, Laser-Induced Graphene from Polyimide and Polyethersulfone Precursors as a Sensing Electrode in Anodic Stripping Voltammetry, *ACS Appl. Mater. Interfaces*, 2020, **12**(43), 48511–48517, DOI: **10.1021/acsami.0c11725**.

66 X. Lin, Z. Lu, W. Dai, B. Liu, Y. Zhang, J. Li and J. Ye, Laser Engraved Nitrogen-Doped Graphene Sensor for the Simultaneous Determination of Cd(II) and Pb(II), *J. Electroanal. Chem.*, 2018, **828**, 41–49, DOI: **10.1016/j.jelechem.2018.09.016**.

67 Z. Lu, X. Lin, J. Zhang, W. Dai, B. Liu, G. Mo, J. Ye and J. Ye, Ionic Liquid/Poly-l-Cysteine Composite Deposited on Flexible and Hierarchical Porous Laser-Engraved Graphene Electrode for High-Performance Electrochemical Analysis of Lead Ion, *Electrochim. Acta*, 2019, **295**, 514–523, DOI: **10.1016/j.electacta.2018.10.176**.

68 X. Lin, Z. Lu, Y. Zhang, B. Liu, G. Mo, J. Li and J. Ye, A Glassy Carbon Electrode Modified with a Bismuth Film and Laser Etched Graphene for Simultaneous Voltammetric Sensing of Cd(II) and Pb(II), *Microchim. Acta*, 2018, **185**(9), 438, DOI: **10.1007/s00604-018-2966-4**.